Distributed Beamforming for Magnetic Induction Based Body Area Sensor Networks

S. Kisseleff*, I. F. Akyildiz**, and W. Gerstacker*
* Institute for Digital Communications, Friedrich-Alexander-Universität (FAU) Erlangen-Nürnberg, Germany
{steven.kisseleff, wolfgang.gerstacker}@fau.de
** Broadband Wireless Networking Lab, Georgia Institute of Technology, USA, ian@ece.gatech.edu

***Abstract*—Body Area Sensor Networks (BASNs) are a challenging research area with applications in healthcare and entertainment. Due to the importance of the target applications in the daily life, BASNs are a promising candidate for being included into the future Internet of Things (IoT). In particular, the data gathering of the human activity may help customizing the services provided by the IoT and thus dramatically improve the IoT user experience.**
Magnetic Induction (MI) based communication is known in the context of wireless power transfer (WPT), near-field communication (NFC), and wireless sensor networks (WSNs) in challenging environments. In this approach, induction coils are utilized as antennas in the sensor nodes.
Distributed beamforming is a well-known technique, that has been thoroughly investigated in the past. Here, the basic idea is to align the phases of signals from different sensor nodes in such a way that a virtual multiple-input multiple-output (MIMO) system with favorable properties is created. For example, this strategy may lead to an improved directionality of the transmitted signals and increase the data rate. In this work, we analyze the potential of the distributed beamforming based MI-BASNs. We observe a significant increase of the data rate for the proposed distributed beamforming compared to our selected baseline scheme.

I. Introduction

Implantable or wearable wireless sensor networks (WSNs) have gained an increased attention in the recent years. Such WSNs are frequently called body area sensor networks (BASNs), which is the term we use in the following. The most intuitive applications of BASNs refer to a wide spectrum of medical services in the healthcare, in particular for the monitoring purposes. Furthermore, the recent advances in the development of entertainment systems require a more detailed interaction with the human body, which could be efficiently established via BASNs. For a deeper insight, we refer to [1], [2]. Due to a more precise information about the human behavior provided by BASNs, these schemes are very promising in the context of the upcoming Internet of Things (IoT). In particular, the use of BASNs may help to customize and adapt the IoT services to the individual needs of the users. This has further motivated an extensive research in the area of BASNs, especially from the perspective of wireless communications.

Magnetic induction (MI) based transmissions are well known in the context of near-field communications (NFC) [3], wireless power transfer (WPT) [4], and WSNs in challenging environments [5]. This method of signal transmission utilizes quasi-static magnetic fields generated by induction coils instead of electromagnetic waves. The major benefit of MI based signal propagation compared to the traditional RF techniques is due to its low vulnerability against additional attenuation and distortion in conductive medium, cf. e.g. [5]. Due to the non-vanishing electrical conductivity of the human body [6], the body area can be viewed as a challenging environment for RF communication [7]. Hence, MI-BASNs have been investigated in multiple previous works, e.g. [8], [9], where the potential of this technology has been revealed in terms of channel capacity, power efficiency, and bit error rate. In addition, the recent developments of magnetic multiple-input multiple-output (MIMO) systems ([10], [11]) have indicated a way to further improve the overall system efficiency and performance of MI based communication systems.

Distributed beamforming is a well-known technique, which is particularly used in general WSNs in order to establish a robust uplink transmission towards a central sink node, cf. e.g. [12]. This technique utilizes a virtual MIMO system created based on the distributed sensor nodes, which can synchronize their transmissions and align their signal phases. Hence, a beamforming gain can be realized, which dramatically improves the signal quality and data rate. For this, the signal transmission is typically split in two steps. At first, the sensors exchange the data to be transmitted, which is then known to all sensors, such that the whole network can be viewed as one transmitter with multiple antennas/coils. In the second step, this transmitter creates a signal beam in the direction of the sink node. Of course, the distributed beamforming can only be established, if all nodes are perfectly synchronized with each other, which is a challenging task in practice. In [12], the impact of an imperfect synchronization on the beamforming is investigated. In this work, we analyze the potential of distributed beamforming for MI based transmissions under optimal conditions including a genie-aided knowledge of the channel state and a perfect synchronization of all sensor nodes. All system parameters are assumed to be perfectly known to all nodes including the sink node. Hence, a practical implementation may show some performance degradation compared to our theoretical results, which may be viewed as upper performance limits.

A distributed beamforming (sometimes also called virtual

This work was supported by the German Research Foundation (Deutsche Forschungsgemeinschaft, DFG) under Grant No. GE 861/4-2.

978-1-5090-1328-9/16/$31.00 ©2016 IEEE

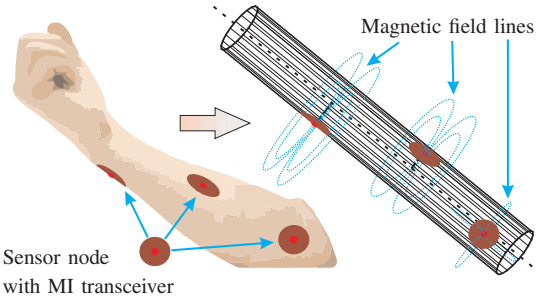

Fig. 1. Example of sensor deployment on a human arm and its schematic representation. Three sensors are attached to the skin. The orientation of MI transceivers corresponds to the respective radial directions of the arm.

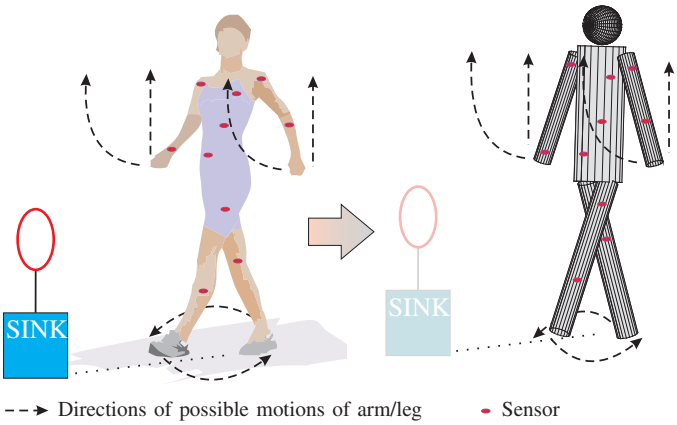

Fig. 2. Example of a BASN attached to a human body and a wirelessly connected sink node (left); corresponding simplified model of human body with identical distribution of sensor nodes (right).

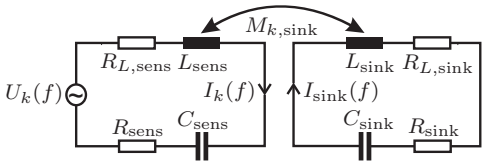

Fig. 3. Magnetic coupling between resonant circuits of node 'k' and sink node.

MIMO or multisensor network) approach can be also applied in BASNs, as shown in [13], where an ultrawideband (UWB) MIMO system corresponding to a BASN infrastructure has been analyzed. The resulting spatially correlated channels have been extensively characterized. Another relevant study is provided in [14], where antenna diversity in an UWB based BASN has been investigated for the off-body scenario, which is very similar to the scenario described above (uplink transmissions to a central sink node). In this work, we apply the idea of distributed beamforming to MI-BASNs, where the transmission channels, however, have substantially different properties compared to traditional BASNs, which does not allow to apply the results from [13] and [14] to our problem. The remainder of this paper is organized as follows. Section II describes the system model, which includes the influence of the human body on the signal transmission between MI transceivers. The use of distributed beamforming in MI-BASNs is presented in Section III. Section IV provides numerical results and Section V concludes the paper.

II. System Model

In this work, N_{nodes} sensor nodes are assumed to be deployed on the surface of the human body. The position of these nodes can be random, however, the orientation of the MI transceivers is not random. In a practical MI-BASN, each coil can only be deployed in such a way, that its axis corresponds to the radial direction of the surface it is placed on (away from the respective body part), see Fig. 1. Otherwise, the nodes may disturb the natural motion of the respective body part or might even be accidentally detached when hitting other body parts or clothes. Hence, the typical assumption of a perfect alignment or equal orientation of the coil axes is not valid in general. Furthermore, the varying orientation of coils among the nodes leads to phase shifts, such that simultaneous transmissions may add destructively rather than constructively in some cases.

Fig. 2 shows an example of multiple sensor nodes attached to a human body. For simplicity, we model the nodes' positions as random points on the surface of the respective cylinder, which represents one of the arms, legs, or the torso. In principle, this model can be extended by multiple cylinders representing elbows, knees, fingers, etc. However, this would substantially increase the system complexity. Furthermore, in case of sensor mobility the position deviation should not be modeled as a random and uncorrelated change (as typically assumed for mobile WSNs), since the on-body nodes are moved by the body parts they are attached to, i.e., a small cluster of nodes that belong to the same body part will move along the trajectory of the respective body part.

As mentioned earlier, we assume that the sensed information is transmitted to a central sink node, which is placed in a reasonable distance to the human body. Furthermore, for simplicity, we assume that all MI transceivers placed in the body area have identical structure and system parameters. In particular, one of the crucial requirements dictated by the relevant applications is the small size of the sensors. For the sink node, this requirement can be neglected, since it is not attached to the human body. In the following, we add a subscript 'sens' to the system parameters of the sensors deployed on the human body and a subscript 'sink' to the system parameters of the sink node, respectively.

Each circuit includes a magnetic antenna (air core coil) with inductivity L_{sens} (or L_{sink}), a capacitor with capacitance C_{sens} (or C_{sink}), a resistor R_{sens} (or R_{sink}), which stands for the copper wire resistance, and a load resistor $R_{L,\text{sens}}$ (or $R_{L,\text{sink}}$), which is employed for the signal reception. The capacitances C_{sens} and C_{sink} are selected to make the circuit resonant at the given resonance frequency $f_0 = \frac{1}{2\pi\sqrt{L_{\text{sens}}C_{\text{sens}}}} = \frac{1}{2\pi\sqrt{L_{\text{sink}}C_{\text{sink}}}}$. A simple MI link between an on-body sensor node and the sink node is shown in Fig. 3. The inductivity of the respective coils is given by [5]

$$L_{\text{sens/sink}} = \frac{1}{2}\mu\pi N^2_{\text{sens/sink}} a_{\text{sens/sink}}, \tag{1}$$

where $N_{\text{sens/sink}}$ stands for the number of windings of sensor nodes and sink, respectively. $a_{\text{sens/sink}}$ represents the radius of the coils of sensor nodes and sink, repectively. In addition, μ is the permeability of the medium. The copper resistance of the coil wires can be determined via

$$R_{\text{sens/sink}} = \rho \cdot \frac{2\, a_{\text{sens/sink}} N_{\text{sens/sink}}}{r_w^2}, \tag{2}$$

where $\rho \approx 1.678 \cdot 10^{-2}\ \Omega{\cdot}\text{mm}^2/\text{m}$ is the copper resistivity and r_w is the radius of the wire. Due to the small size of sensor nodes and the resulting weak coupling between coils, the optimal values for $R_{L,\text{sens}}$ and $R_{L,\text{sink}}$ are equal to R_{sens} and R_{sink}, respectively, as suggested by [4]. The induced voltage is related to the coupling between the coils, which is determined by the mutual inductance denoted as $M_{k,\text{sink}}$ for the link between an on-body sensor node k and the sink node, and by the mutual inductance $M_{k,l}$ for the link between two on-body sensor nodes k and l. By combining results from previous works (in particular [15] and [5]), we obtain

$$M_{k,\text{sink}} = \mu\pi N_{\text{sens}} N_{\text{sink}} \frac{a_{\text{sens}}^2 a_{\text{sink}}^2}{4 r_{k,\text{sink}}^3} \cdot J_{k,\text{sink}} \cdot G_{k,\text{sink}}, \tag{3}$$

$$M_{k,l} = \mu\pi N_{\text{sens}}^2 \frac{a_{\text{sens}}^4}{4 r_{k,l}^3} \cdot J_{k,l} \cdot G_{k,l}, \tag{4}$$

where $r_{k,l/\text{sink}}$ denotes the distance between the coils k and l or sink, respectively. For determining the polarization factor $J_{k,l/\text{sink}}$, we model the magnetic field of the coils as magnetic dipoles in a three-dimensional space, resulting in [15]

$$\begin{aligned} J_{k,l/\text{sink}} = {} & 2\sin(\theta_k)\sin(\theta_{l/\text{sink}}) \\ & + \cos(\theta_k)\cos(\theta_{l/\text{sink}})\cos(\phi_{k,l/\text{sink}}), \end{aligned} \tag{5}$$

where θ_k and $\theta_{l/\text{sink}}$ are the angles between the respective coil radial direction and the line connecting the two corresponding coil centers, respectively. $\phi_{k,l/\text{sink}}$ is the angle difference between the corresponding coil axes in the plane, which is orthogonal to the direction of transmission. $G_{k,l/\text{sink}}$ represents an additional attenuation for the link between node k and l/sink due to the conductive medium (human body in this work), which mainly influences the links between the on-body nodes. The sink node is placed in the free space and in considerable distance from the body, such that it can be accessed via line-of-sight (LoS) from most of the sensor nodes. Hence, $G_{k,\text{sink}} = 1, \forall k$ is assumed. Furthermore, regarding the attenuation of signal transmission between the on-body sensors, the magnetic field lines propagate partially through the body and partially through the air (see Fig. 1), which can be approximately modeled as field propagation at the surface of a dense medium, resulting in [16]

$$G_{k,l} = \frac{2}{\gamma_{k,l}^2}\left(9 - \left(9 + 9\gamma_{k,l} + 4\gamma_{k,l}^2 + \gamma_{k,l}^3\right)\mathrm{e}^{-\gamma_{k,l}}\right), \tag{6}$$

with $\gamma_{k,l} = r_{k,l}\sqrt{\pi f_0 \mu \sigma_{k,l}}$, where $\sigma_{k,l}$ is the body conductivity between the coils k and l. This parameter can be obtained via a detailed modeling of all body components, e.g., bones, muscles, etc. [6]. Alternatively, an average value has been assumed in [17], where $\sigma_{k,l} = 0.2$ S/m $\forall k, l$. In this work, we use the latter option, which significantly reduces the complexity of system modeling.

Of course, with the above mentioned simplifications, the resulting signal propagation model is not exact. However, more precise system models for MI-BASNs have not been presented in the literature so far, since either the influence of the conductive property of the human body or a realistic deployment of the sensor nodes on the surface of the respective body parts has been neglected. Hence, the presented system model is one of the contributions of this work.

The inner impedance of the on-body circuits is given by

$$Z_{\text{in,sens}}(f) = R_{\text{sens}} + j2\pi f L_{\text{sens}} + \frac{1}{j2\pi f C_{\text{sens}}} + R_{L,\text{sens}}, \tag{7}$$

and the inner impedance of the sink circuit is

$$Z_{\text{in,sink}}(f) = R_{\text{sink}} + j2\pi f L_{\text{sink}} + \frac{1}{j2\pi f C_{\text{sink}}} + R_{L,\text{sink}}. \tag{8}$$

In addition, we define $Z_{k,l}(f) = j2\pi f M_{k,l}$, $k \neq l$, and $Z_{k,\text{sink}}(f) = j2\pi f M_{k,\text{sink}}$, $\forall k$.

For simplicity, we assume that each sensor node utilizes a non-frequency-selective transmit filter $h(t)$ within a given frequency band B, such that for each channel use the input voltage to each transmitter circuit is identical for all frequencies within the given transmission band. This transmit filter corresponds to a root-raised cosine (RRC) filter with roll-off factor $\beta = 0$. In time domain, the complex-valued transmit voltage of circuit k is given by

$$u_k(t) = \alpha_k \sum_{m=-\infty}^{\infty} s_k[m] h(t - mT), \tag{9}$$

where a sequence of symbols $s_k[m]$ spaced by the symbol duration $T = \frac{1}{B}$ is fed into the transmit filter $h(t)$, which generates the voltage signal $u_k(t)$. In (9), α_k is a voltage amplification factor. Furthermore, we assume that $\mathcal{E}\{|s_k[m]|^2\} = 1$, $\forall k$ holds, where $\mathcal{E}\{\cdot\}$ denotes the expectation operator. In frequency domain, we consider the complex-valued amplitudes $U_k(f) = \mathcal{F}\{u_k(t)\}$ and $I_k(f) = \mathcal{F}\{i_k(t)\}$ of the voltages $u_k(t)$ and currents $i_k(t)$, respectively, of the kth circuit. Here, $\mathcal{F}\{\cdot\}$ denotes the Fourier transform operator. Furthermore,

$$H(f) = \mathcal{F}\{h(t)\} = \begin{cases} 1, & f_0 - \frac{1}{2}B \leq f \leq f_0 + \frac{1}{2}B \\ 0, & \text{else} \end{cases} \tag{10}$$

is assumed. For the sink node, we set the input voltage to zero, i.e. $U_{\text{sink}}(f) \equiv 0$, since it only collects the information.[1]

In order to calculate the currents in all circuits of the coupled network, we stack all input voltages of the sensor nodes in a vector $\mathbf{U}_{\text{sens}}(f) = [U_1(f), \ldots, U_{N_{\text{nodes}}}(f)]^T$ and solve a set of voltage equations

$$\begin{bmatrix} \mathbf{Z}_{\text{sens}}(f) & \mathbf{Z}_{Ch}(f) \\ \mathbf{Z}_{Ch}^T(f) & Z_{\text{in,sink}}(f) \end{bmatrix} \cdot \begin{bmatrix} \mathbf{I}_{\text{sens}}(f) \\ I_{\text{sink}}(f) \end{bmatrix} = \begin{bmatrix} \mathbf{U}_{\text{sens}}(f) \\ 0 \end{bmatrix}. \tag{11}$$

[1] $U_{\text{sink}}(f) \equiv 0$ refers only to the useful signal. However, the noise signals may occur in the receiver circuit of the sink node in terms of additional voltage sources. Its modeling will be addressed later.

Here, $\mathbf{I}_{\text{sens}}(f)$ denotes a vector comprising the Fourier transforms of the currents of the on-body node circuits. The matrices $\mathbf{Z}_{\text{sens}}(f)$ and $\mathbf{Z}_{Ch}(f)$ contain complex impedances and are defined in the following:

$$\mathbf{Z}_{\text{sens}}(f) = \begin{bmatrix} Z_{\text{in,sens}}(f) & Z_{2,1}(f) & \cdots & Z_{1,\text{nodes}}(f) \\ Z_{1,2}(f) & Z_{\text{in,sens}}(f) & \cdots & Z_{2,\text{nodes}}(f) \\ \vdots & \vdots & \ddots & \vdots \\ Z_{1,\text{nodes}}(f) & Z_{2,\text{nodes}}(f) & \cdots & Z_{\text{in,sens}}(f) \end{bmatrix}, \quad (12)$$

$$\mathbf{Z}_{Ch}(f) = [Z_{1,\text{sink}}(f), \ldots, Z_{N_{\text{nodes}},\text{sink}}(f)]^T. \quad (13)$$

By inverting the impedance matrix in (11) using [18], we obtain similarly to [11]

$$\begin{aligned} \mathbf{I}_{\text{sens}}(f) &= \left(\mathbf{Z}_{\text{sens}}(f) - \mathbf{Z}_{Ch}(f)\mathbf{Z}_{Ch}^T(f)Z_{\text{in,sink}}^{-1}(f)\right)^{-1}\mathbf{U}_{\text{sens}}(f) \\ &= \mathbf{A}(f)\mathbf{U}_{\text{sens}}(f), \end{aligned} \quad (14)$$

$$\begin{aligned} I_{\text{sink}}(f) &= -Z_{\text{in,sink}}^{-1}(f)\mathbf{Z}_{Ch}^T(f)\mathbf{A}(f)\mathbf{U}_{\text{sens}}(f) \\ &= \mathbf{C}(f)\mathbf{U}_{\text{sens}}(f), \end{aligned} \quad (15)$$

with implicit definitions of $\mathbf{A}(f)$ and $\mathbf{C}(f)$. In addition, we define a scalar

$$D(f) = \left(Z_{\text{in,sink}}(f) - \mathbf{Z}_{Ch}^T(f)\mathbf{Z}_{\text{sens}}^{-1}(f)\mathbf{Z}_{Ch}(f)\right)^{-1}, \quad (16)$$

which is used for mapping of the noise voltage from the receiver circuit of the sink on the current of the sink and will be discussed in the context of noise power calculation.

Due to the small size of on-body sensor nodes and the propagation through a conductive medium causing additional attenuation, the strength of the magnetic field produced by the sensors and correspondingly the coupling between the sensors is very weak. Hence, $\mathbf{A}(f)$ can be approximated by $\mathbf{A}(f) \approx \mathbf{I} \cdot Z_{\text{in,sens}}^{-1}(f)$, where $\mathbf{I}$ is the identity matrix of dimension $N_{\text{nodes}} \times N_{\text{nodes}}$. As argued in [19], the optimization of MI communication systems with respect to solely the active transmit power [4] is not reasonable, since the influence of the reactive power on the system stability is not negligible. Instead, we consider the apparent power, which incorporates both the active and the reactive powers [20]. Hence, the sum transmit power spectral density (PSD) of all sensor nodes can be given by [11]

$$\begin{aligned} P_t(f) &= \mathcal{E}\{|\mathbf{I}_{\text{sens}}(f)|^T |\mathbf{U}_{\text{sens}}(f)|\} \\ &= \mathcal{E}\{|\mathbf{A}(f)\mathbf{U}_{\text{sens}}(f)|^T |\mathbf{U}_{\text{sens}}(f)|\} \\ &\approx \mathcal{E}\{\mathbf{U}_{\text{sens}}^H(f)|Z_{\text{in,sens}}^{-1}(f)|\mathbf{U}_{\text{sens}}(f)\} \\ &= \mathcal{E}\{\mathbf{U}_{\text{sens}}^H(f)\mathbf{U}_{\text{sens}}(f)\}|Z_{\text{in,sens}}^{-1}(f)|. \end{aligned} \quad (17)$$

Since the data symbols $s_k[m]$, $\forall k, m$ are uncorrelated, we obtain $\mathcal{E}\{\mathbf{U}_{\text{sens}}^H(f)\mathbf{U}_{\text{sens}}(f)\} = \sum_{k=1}^{N_{\text{nodes}}} \alpha_k^2 |H(f)|^2$. Thus, the total power consumed by the sensor nodes is obtained

$$P_{\text{consumed}} \approx \sum_{k=1}^{N_{\text{nodes}}} \alpha_k^2 \int_{f_0-0.5B}^{f_0+0.5B} \left|Z_{\text{in,sens}}^{-1}(f)\right| \mathrm{d}f, \quad (18)$$

where the assumption of a rectangular transmit PSD has been used. Similarly, for the sum received active PSD at the load impedance of the sink node, we obtain

$$\begin{aligned} P_r(f) &= \mathcal{E}\{|I_{\text{sink}}(f)|^2 R_{L,\text{sink}}\} \\ &= \mathcal{E}\{\mathbf{U}_{\text{sens}}^H(f)\mathbf{C}^H(f)\mathbf{C}(f)\mathbf{U}_{\text{sens}}(f)R_{L,\text{sink}}\} \\ &= \sum_{k=1}^{N_{\text{nodes}}} \alpha_k^2 |H(f)|^2 \mathbf{e}_k^H \mathbf{C}^H(f)\mathbf{C}(f)\mathbf{e}_k R_{L,\text{sink}}, \end{aligned} \quad (19)$$

where $\mathbf{e}_k = [0, \ldots, 0, 1, 0, \ldots, 0]^T$ with the '1' at the kth position. Typically, the transmitted data is corrupted by noise and interference caused by other systems (in particular by other MI based transmissions). We model the noise source in each resonant circuit as a voltage source, which provides an additive white Gaussian noise (AWGN) with the PSD N_0. Since this noise propagates through the whole network, the receive noise that arrives at the load impedance of the sink consists of the contribution from the sink node itself and the contributions from the sensor nodes. The latter noise signals are heavily attenuated and can typically be neglected in the performance analysis, if the distance between the sensor nodes and the sink node is not too small [15]. Hence, the sum noise PSD is approximately given by

$$N(f) \approx N_0 |D(f)|^2 R_{L,\text{sink}}. \quad (20)$$

III. Distributed Beamforming

In this section, a distributed beamforming based approach for MI-BASNs is introduced. For comparison, we describe also a baseline scheme, where no distributed beamforming is applied and instead all sensor nodes transmit their data one by one. This baseline scheme is referred to as individual transmissions.

A. Individual Transmissions

In the following, we focus on the signal transmissions within one burst consisting of N_{nodes} sequential time slots. We assume that each time slot is occupied by transmissions of only one sensor node. Hence, in each time slot $k \in \{1, \ldots, N_{\text{nodes}}\}$ of burst m a voltage vector $\mathbf{U}_{\text{sens},k}(f) = \alpha_k H(f) s_k[m] \, \mathrm{e}^{-j2\pi f m T} \, \mathbf{e}_k$ is transmitted, where α_k is the voltage amplification, which ensures that the consumed power according to (18) fulfills the system requirements. Obviously, the assumption $\alpha_k = \alpha$, $\forall k$ is reasonable, since all sensors contain the same set of passive elements and have identical structure. The total transmit power for all time slots is denoted by P, such that the transmit power in each time slot is $\frac{P}{N_{\text{nodes}}}$. Hence, we obtain using (17) and $\mathcal{E}\{\mathbf{U}_{\text{sens},k}^H(f)\mathbf{U}_{\text{sens},k}(f)\} = \alpha^2 |H(f)|^2$:

$$P_{\text{consumed}} = \alpha^2 \int_{f_0-0.5B}^{f_0+0.5B} \left|Z_{\text{in,sens}}^{-1}(f)\right| \mathrm{d}f = \frac{P}{N_{\text{nodes}}} \quad (21)$$

and correspondingly

$$\alpha = \sqrt{\frac{P}{N_{\text{nodes}} \int_{f_0-0.5B}^{f_0+0.5B} \left|Z_{\text{in,sens}}^{-1}(f)\right| \mathrm{d}f}}. \quad (22)$$

As known from the literature [21], the maximum achievable data rate can be calculated via Shannon's formula. Hence, in case of continuous transmission from node k, the data rate $C_{\mathrm{data},k}$ can be determined using (19) and (20)

$$C_{\mathrm{data},k} = \int_{f_0-0.5B}^{f_0+0.5B} \log_2\left(1 + \frac{\mathbf{e}_k^H \mathbf{C}^H(f)\mathbf{C}(f)\mathbf{e}_k \alpha^2}{N_0 \left|D(f)\right|^2}\right) \mathrm{d}f. \quad (23)$$

However, since each node transmits only in every kth time slot and remains silent in all other time slots, the resulting sum rate C_{baseline} of all sensor nodes has to be normalized:

$$C_{\mathrm{baseline}} = \frac{1}{N_{\mathrm{nodes}}} \sum_{k=1}^{N_{\mathrm{nodes}}} C_{\mathrm{data},k}. \quad (24)$$

B. Beamforming

In order to establish a synchronized MIMO system for simultaneous transmissions of identical information from multiple sensor nodes, two steps are needed. In the first step, the sensor nodes exchange the information to be transmitted to the sink. In the second step, all on-body sensors are synchronized and transmit the information acquired in the first step simultaneously. By optimizing the phases and amplitudes of the individual signals, an MI beam can be formed. For a fair comparison with the baseline scheme from Section III-A, the consumed power in each step is set to $0.5P$. Hence, in each time slot k of the second step of burst m, a voltage vector $\mathbf{U}_{\mathrm{beam},k}(f) = \sqrt{0.5}\alpha H(f) s_k[m]\, \mathrm{e}^{-j2\pi f m T}\, \mathbf{x}_{\mathrm{beam}}$ is transmitted, where $\mathbf{x}_{\mathrm{beam}}$ is the beamforming vector with $\|\mathbf{x}_{\mathrm{beam}}\|_2 = 1$, and α is obtained using (22).

For simplicity, we assume that all on-body nodes can perfectly decode all messages from the other nodes. This assumption is justified due to relatively small distances between the on-body nodes, such that the coupling between coils is strong enough to provide a sufficient signal quality for reliable detection and decoding. Hence, we focus on the sum rate, which is obtained using signals at the sink from the first and the second step. Of course, the second step is more efficient than the first step due to the beamforming gain, however, in order to investigate the maximum data rate we employ the signals obtained from both steps.

In fact, the exchange of information among the nodes in the first step can be also viewed as individual transmissions towards the sink node and utilized in order to improve the signal quality by coherently combining these signals with the respective signals from the second step. For this, we define[2]

$$\mathrm{SNR}_{1,k}(f) = \frac{\mathbf{e}_k^H \mathbf{C}^H(f)\mathbf{C}(f)\mathbf{e}_k \alpha^2 \left|H(f)\right|^2}{2N_0 \left|D(f)\right|^2},\ 1 \le k \le N_{\mathrm{nodes}}, \quad (25)$$

for the first step and

$$\mathrm{SNR}_{2,k}(f) = \frac{\mathbf{x}_{\mathrm{beam}}^H \mathbf{C}^H(f)\mathbf{C}(f)\mathbf{x}_{\mathrm{beam}} \alpha^2 \left|H(f)\right|^2}{2N_0 \left|D(f)\right|^2}, \quad 1 \le k \le N_{\mathrm{nodes}}, \quad (26)$$

for the second step. In the following, we focus on the optimization of $\mathbf{x}_{\mathrm{beam}}$.

At the sink node, we employ matched filters for both steps matched to the corresponding overall channel transfer function and noise PSD. Hence, using this optimal approach of maximum ratio combining (MRC), the signals of both steps are combined coherently. The resulting combined spectral signal-to-noise ratio (SNR) of both steps can be given by

$$\mathrm{SNR}_{\mathrm{MRC},k}(f) = \mathrm{SNR}_{1,k}(f) + \mathrm{SNR}_{2,k}(f). \quad (27)$$

The sum rate of the beamforming based approach can be given by[3]

$$C_{\mathrm{beam}} = \frac{1}{2N_{\mathrm{nodes}}} \sum_{k=1}^{N_{\mathrm{nodes}}} \int_{f_0-0.5B}^{f_0+0.5B} \log_2\left(1 + \mathrm{SNR}_{\mathrm{MRC},k}(f)\right) \mathrm{d}f. \quad (28)$$

The optimum beamforming vector $\mathbf{x}_{\mathrm{beam}}$ is found by solving the optimization problem

$$\max_{\mathbf{x}_{\mathrm{beam}}} \quad C_{\mathrm{beam}} \quad (29)$$

$$\text{s.t.} \quad \mathbf{x}_{\mathrm{beam}}^H \mathbf{x}_{\mathrm{beam}} = 1. \quad (30)$$

This problem is non-concave [22]. Hence, no closed-form or globally optimum solution can be given. However, the Lagrangian of this problem can be formulated as

$$L(\mathbf{x}_{\mathrm{beam}}) = C_{\mathrm{beam}} + \nu\left(\mathbf{x}_{\mathrm{beam}}^H \mathbf{x}_{\mathrm{beam}} - 1\right), \quad (31)$$

where ν denotes the Lagrange multiplier. A locally optimum vector $\mathbf{x}_{\mathrm{beam}}$ fulfills $\frac{\partial L(\mathbf{x}_{\mathrm{beam}})}{\partial \mathbf{x}_{\mathrm{beam}}^*} = \mathbf{0}$. Hence, using (25)-(28) we obtain a non-linear eigenvalue problem similar to [22]

$$\sum_{k=1}^{N_{\mathrm{nodes}}} \int_{f_0-0.5B}^{f_0+0.5B} \frac{\frac{\mathbf{C}^H(f)\mathbf{C}(f)}{\left|D(f)\right|^2}\, \mathrm{d}f}{\left(1 + \mathrm{SNR}_{\mathrm{MRC},k}(f)\right)}\, \mathbf{x}_{\mathrm{beam}} = \tilde{\mu}\, \mathbf{x}_{\mathrm{beam}} \quad (32)$$

with eigenvalue $\tilde{\mu}$. In the following, we propose a gradient algorithm for calculation of the optimal beamforming vector.

C. Gradient Algorithm

The starting point of the algorithm is a suitable vector $\mathbf{x}_{\mathrm{beam},0}$, where $\mathbf{x}_{\mathrm{beam},n}$ represents the state of the beamforming vector at the end of the nth iteration. In each iteration of the algorithm, we calculate the direction of the gradient by

$$grad_n(C_{\mathrm{beam}}) = \sum_{k=1}^{N_{\mathrm{nodes}}} \int_{f_0-0.5B}^{f_0+0.5B} \frac{\frac{\mathbf{C}^H(f)\mathbf{C}(f)}{\left|D(f)\right|^2}\, \mathrm{d}f \cdot \mathbf{x}_{\mathrm{beam},n-1}}{\left(1 + \mathrm{SNR}_{\mathrm{MRC},k}(f)\right)}. \quad (33)$$

Using (33), the beamforming vector is updated via

$$\tilde{\mathbf{x}}_{\mathrm{beam},n} = \mathbf{x}_{\mathrm{beam},n-1} + \delta\, \frac{grad_n(C_{\mathrm{beam}})}{\|grad_n(C_{\mathrm{beam}})\|_2}, \quad (34)$$

where δ is a suitable adaptation step size. According to our observations (based on the numerical results provided in

[2]Factor 2 in the denominator of (25) and (26), respectively, results from the reduced transmit power ($0.5P$) in each step compared to (21) as mentioned earlier.

[3]Factor $\frac{1}{2}$ in (28) results from the fact that the data packets reach the sink node after two steps, which are assumed to be of equal duration. Since both steps are used to transmit only N_{nodes} data packets, the bandwidth efficiency and the sum rate reduces by 50% compared to the continuous beamforming transmissions, respectively.

Section IV), $\delta = 0.1$ seems to be a good choice. In order to satisfy the transmit power constraint, the resulting vector $\tilde{\mathbf{x}}_{\mathrm{beam},n}$ is normalized to unit norm by

$$\mathbf{x}_{\mathrm{beam},n} = \frac{\tilde{\mathbf{x}}_{\mathrm{beam},n}}{\|\tilde{\mathbf{x}}_{\mathrm{beam},n}\|_2}. \tag{35}$$

A suitable stopping condition is $1 - \left|\mathbf{x}_{\mathrm{beam},n}^H \mathbf{x}_{\mathrm{beam},n-1}\right| < \epsilon$ with a small ϵ, e.g. $\epsilon = 10^{-3}$. Using the beamforming vector from the last iteration, C_{beam} is calculated. According to our observations, the algorithm converges within $n < 10$.

IV. Numerical Results

As mentioned in Section II, we model the deployment of sensor nodes on the body using 5 cylinders representing torso (radius 30 cm, height 70 cm), legs (radius 5.5 cm, length 85 cm each), and arms (radius 4.5 cm, length 60 cm each), respectively. Furthermore, for a more realistic scenario, we add a small gap of 5 cm between torso and each of the arms, which represents a shoulder and allows for a correct rotation of the arms. We assume that each sensor can be placed either on the torso, on one of the legs, or on one of the arms with equal probability. The arms and legs can be rotated according to Fig. 2. For each simulation point, we consider 100 scenarios with a different set of sensors and different positions of all body parts. This allows for a realistic conclusion on the average performance of the network. The sink node is placed at the height of the waistline and rotated towards the body. This scenario is typical for the sport activities in gym, where the position of the body does not change, while the body parts move. In the discussion below, we investigate the data rate for different distances between the center of the body at the height of the waistline and the sink position, which refers to the actual distance between the body and the sink. Furthermore, since MI based communication can be viewed as a special case of passive radio frequency identification (RFID), we select a carrier/resonance frequency $f_0 = 13.56$ MHz and a bandwidth $B = 14$ kHz according to the respective standards ISO 14443/15693. The available transmit power P may increase with increasing number of sensors, such that we select $P = N_{\mathrm{nodes}} \cdot 100\ \mu$W. We assume the following parameters: $N_{\mathrm{sens}} = 1$, $a_{\mathrm{sens}} = 5$ mm, $N_{\mathrm{sink}} = 10$, $a_{\mathrm{sink}} = 5$ cm, $\mu = 4\pi \cdot 10^{-7}$ H/m, and $r_w = 1$ mm.

We start with the analysis of the sum rate, see Fig. 4. In case of low SNR (Fig. 4a)), the beamforming method dramatically improves the system performance. This improvement is obviously increasing with increasing number of sensor nodes. With increasing SNR, the rate gain vanishes, such that the baseline scheme based on individual transmissions outperforms the distributed beamforming, see Fig. 4b). This situation occurs if the sink node is placed in a close neighborhood of the body or in case of a low number of sensors, such that the resulting beamforming gain cannot compensate the aforementioned reduced bandwidth efficiency (factor $\frac{1}{2}$ in (28)). However, with increasing number of deployed sensors, the intersection of the beamforming curve and the baseline curve moves towards shorter distances to the sink node. Hence, with a sufficient

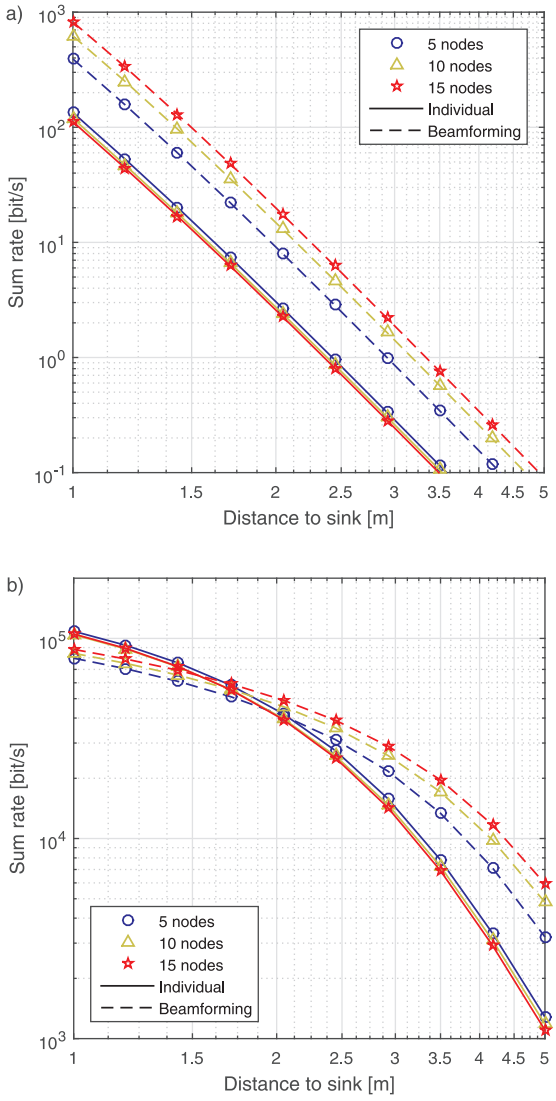

Fig. 4. Average sum rate vs. distance between body and sink for different noise PSDs. a) $N_0 = 10^{-10} V^2 s$; b) $N_0 = 10^{-15} V^2 s$.

size of the network (e.g. $N_{\mathrm{nodes}} = 10$), substantial gains with respect to the sum rate can be observed even for a distance below 3 m.

Thus, the system performance of the distributed beamforming approach depends on the number of sensor nodes. This effect is also illustrated in Fig. 5. Here, the average sum rate is shown for $N_0 = 10^{-15} V^2 s$ and different distances of the body to the sink node (2 m and 4 m). For individual transmissions, we observe a slight decrease of the sum rate with increasing numbers of sensor nodes, which results from the near-field coupling of each sensor node with more and more devices that absorb parts of the generated magnetic field. Hence, less and less power of the useful signal reaches the sink node and the sum rate decreases. Obviously, a significant improvement of the data rate using the beamforming strategy is observed. On average, the rate gain for 2 m is bounded by 48% using 25 nodes. For 4 m, a rate gain of up to 420% can be reached using 25 nodes. These results make the distributed

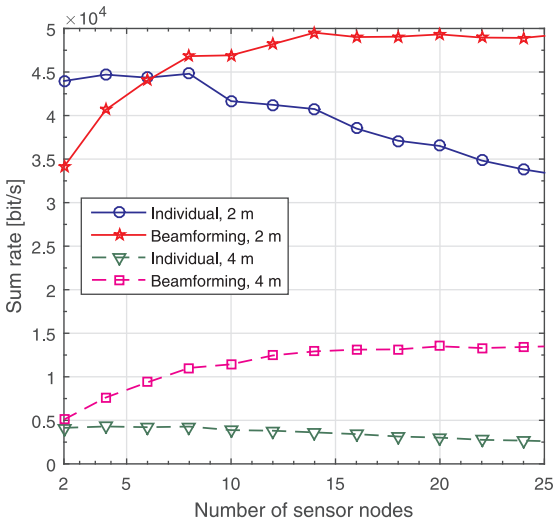

Fig. 5. Average sum rate vs. number of sensor nodes for different distances between body and sink.

beamforming approach a good candidate for MI-BASNs. For transmissions with a distance of 2 m, we observe that the baseline scheme outperforms the distributed beamforming, if only a small number of sensors is employed. However, the rate loss is bounded by 29%, if only 2 nodes are used. Also, taking into account the recent trend of increasing the number of antennas, sensors, users, etc. towards large-scale networks, this situation seems to be unlikely and undesirable for the future BASNs and IoT.

V. Conclusion

In this work, a distributed beamforming approach for transferring sensor data from an MI-BASN to a distant sink node has been presented. We assume that all sensor nodes deployed on the human body are perfectly synchronized. Of course, an imperfect synchronization may significantly reduce the overall system performance. However, the respective analysis is beyond the scope of this work. The distribution of the on-body nodes in the three-dimensional space is modeled as random positions on the surface of the respective cylinder, which can represent an arm, a leg, or a torso. Furthermore, an additional attenuation due to the electrical conductivity of the human body has been taken into account. The system performance of the proposed distributed beamforming is compared with a baseline scheme with individual transmissions and no beamforming in terms of the sum rate. In order to obtain a beamforming solution with maximum sum rate, a gradient based algorithm is utilized, since no closed-form expression can be found. The performance has been evaluated using numerical simulations. The proposed solution shows a substantial increase of the data rate compared to the baseline scheme, especially in the low SNR regime. For very high SNR, i.e., in case of low noise power or very short distance of the BASN to the sink node, the baseline scheme outperforms the distributed beamforming approach. However, in case of larger distances between the body and the sink node, large rate gains of up to 420% can be reached using a sufficient number of sensor nodes.

References

[1] M. Hanson, H. Powell, A. Barth, K. Ringgenberg, B. Calhoun, J. Aylor, and J. Lach, "Body area sensor networks: Challenges and opportunities," *IEEE Computer*, vol. 42, pp. 58–65, January 2009.

[2] S. Movassaghi, M. Abolhasan, J. Lipman, D. Smith, and A. Jamalipour, "Wireless Body Area Networks: A Survey," *IEEE Communications Surveys & Tutorials*, vol. 16, no. 3, pp. 1658–1686, January 2014.

[3] R. Bansal, "Near-field magnetic communication," in *IEEE Antennas and Propagation Magazine*, April 2004.

[4] A. Karalis, J.D. Joannopoulos, and M. Soljacic, "Efficient wireless non-radiative mid-range energy transfer," *Annals of Physics*, vol. 323, pp. 34– 48, January 2008.

[5] Z. Sun and I.F. Akyildiz, "Magnetic induction communications for wireless underground sensor networks," *IEEE Trans. on Antennas and Propag.*, vol. 58, pp. 2426–2435, July 2010.

[6] N. Siauve, R. Scorretti, N. Burais, L. Nicolas, and A. Nicolas, "Electromagnetic fields and human body: a new challenge for the electromagnetic field computation," *The International Journal for Computation and Mathematics in Electrical and Electronic Engineering*, vol. 22, no. 3, pp. 457–469, 2003.

[7] A. Fort, C. Desset, J. Ryckaert, P. De Doncker, L. Van Biesen, and P. Wambacq, "Characterization of the ultra wideband body area propagation channel," in *Proc. of IEEE International Conference on Ultra-Wideband 2005*, September 2005.

[8] J.I. Agbinya and M. Masihpour, "Power equations and capacity performance of Magnetic Induction body area network nodes," in *Proc. of IB2Com*, December 2010.

[9] N. Thilak and R. Braun, "Near field magnetic induction communication in body area network," in *Proc. of ICDCS*, March 2012.

[10] N. Hoang, J.I. Agbinya, and J. Devlin, "FPGA-Based Implementation of Multiple Modes in Near Field Inductive Communication Using Frequency Splitting and MIMO Configuration," *IEEE Trans. on Circuits and Systems I: Regular Papers*, vol. 62, no. 1, pp. 302–310, January 2015.

[11] S. Kisseleff, I.F. Akyildiz, and W.H. Gerstacker, "Beamforming for Magnetic Induction based Wireless Power Transfer Systems with Multiple Receivers," in *Proc. of IEEE Globecom 2015*, December 2015.

[12] R. Mudumbai, G. Barriac, and U. Madhow, "On the Feasibility of Distributed Beamforming in Wireless Networks," *IEEE Trans. on Wireless Communications*, vol. 6, no. 5, pp. 1754–1763, May 2007.

[13] S. van Roy, C. Oestges, F. Horlin, and P. De Doncker, "A Comprehensive Channel Model for UWB Multisensor Multiantenna Body Area Networks," *IEEE Trans. on Antennas and Propag.*, vol. 58, no. 1, pp. 163–170, January 2010.

[14] M. Marinova, A. Thielens, E. Tanghe, L. Vallozzi, G. Vermeeren, W. Joseph, H. Rogier, and L. Martens, "Diversity Performance of Off-Body MB-OFDM UWB-MIMO," *IEEE Trans. on Antennas and Propag.*, vol. 63, no. 7, pp. 3187–3197, July 2015.

[15] S. Kisseleff, I.F. Akyildiz, and W.H. Gerstacker, "Throughput of the Magnetic Induction Based Wireless Underground Sensor Networks: Key Optimization Techniques," *IEEE Trans. on Communications*, vol. 62, no. 12, pp. 4426–4439, December 2014.

[16] J.R. Wait, "Mutual Coupling of Loops Lying on the Ground," *Geophysics Mag.*, vol. 19, pp. 290–296, April 1954.

[17] N. Cho, J. Yoo, S.-J. Song, J. Lee, S. Jeon, and H.-J. Yoo, "The Human Body Characteristics as a Signal Transmission Medium for Intrabody Communication," *IEEE Trans. on Microwave Theory and Techniques*, vol. 55, no. 5, pp. 457–469, May 2007.

[18] D. Bernstein, *Matrix Mathematics*. Princeton University Press, 2005.

[19] N. Tal, Y. Morag, and Y. Levron, "Design of magnetic transmitters with efficient reactive power utilization for inductive communication and wireless power transfer," in *Proc. of IEEE COMCAS*, November 2015.

[20] A. von Meier, *Electric Power Systems: A Conceptual Introduction*. John Wiley & Sons, 2015.

[21] D. Tse and P. Viswanath, *Fundamentals of Wireless Communication*. Cambridge University Press, 2005.

[22] Y.-W. Liang, R. Schober, and W. Gerstacker, "Transmit Beamforming for Frequency-Selective Channels with Decision-Feedback Equalization," *IEEE Trans. on Wireless Communications*, vol. 6, no. 12, pp. 4402–4411, December 2007.